Performance Enhancement of Bistable Piezoelectric Energy Harvesters Using Non-Linear Energy Extraction Circuit

Quentin Demouron, Adrien Morel, David Gibus, Aya Benhemou, Adrien Badel

PERFORMANCE ENHANCEMENT OF BISTABLE PIEZOELECTRIC ENERGY HARVESTERS USING NON-LINEAR ENERGY EXTRACTION CIRCUIT

Quentin Demouron, Adrien Morel, David Gibus, Aya Benhemou and Adrien Badel
Univ. Savoie Mont Blanc, FRANCE

ABSTRACT

Piezoelectric energy harvesters (PEH) require an electronic circuit to rectify their AC voltage in order to supply wireless sensors. In the literature, it has been shown that such electronic circuit can be tuned and optimized in order to enhance the bandwidth and power of linear PEH. However, to date, few works have explored the electrical optimization of non-linear bistable PEH. The present work reports the optimization of the harvested power and bandwidth of bistable PEH by mean of a non-linear energy extraction circuit: the parallel synchronized switch harvesting on inductor (P-SSHI). A simple model of the bistable PEH connected to the P-SSHI circuit has been derived and the closed-form expression of the harvested power has been obtained. The experimental tests, conducted on a custom-made bistable PEH showed that the results are in good agreement with the model, proving its validity. Based on the model, it is shown that the P-SSHI circuit allows to increase the bandwidth (1.6 times) and the harvested power (up to 7.5 times) compared to the standard energy harvesting (SEH) circuit.

KEYWORDS

Piezoelectricity, energy harvesting, non-linear dynamical systems, electromechanical systems, SSHI.

INTRODUCTION

Energy harvesting constitutes a promising approach to power low-consumption wireless sensors. Particularly, vibration energy harvesting is of interest in environments where other energy sources such as solar or thermic energies are not available.

The first PEH that have been proposed in the literature were based on linear mechanical resonators [1]. However, the harvested power with linear PEH drastically decreases if the vibration frequency does not match the resonant frequency of the system [2]. To overcome this limitation, non-linearities were added to the mechanical resonators, allowing the design of broadband non-linear PEH [3][4].

Concerning electrical interfaces for PEH, the first circuit that has been investigated is a rectifier followed by a DC/DC converter [5]. Thereafter, non-linear circuits like synchronous electric charge extraction (SECE), serial switch harvesting on inductor (S-SSHI) or parallel switch harvesting on inductor (P-SSHI) have been proposed in the literature, in order to increase the harvested power. Thanks to a non-linear processing of the piezoelectric voltage, these techniques allow to increase the harvested power as well as the bandwidth of PEH. As illustrated in Fig. 1, all these circuits have been modeled and studied associated with linear PEH. However, to date, few articles focused on the mutual impact and modeling of non-linear circuits combined with non-linear PEH.

In [9], Huguet et al. proposed a numerical and experimental analysis of the mutual influences of SECE circuit combined with bistable PEH. More recently, Wang et al. [10] proposed an analytical modelling and experimental validation of non-linear electrical interfaces applied to non-linear monostable PEH. However, these works did not derive any closed-form expression of the power-frequency response of the PEH, in a simple and physically-insightful way.

In this paper, we propose an analytical model with experimental validation of the P-SSHI circuit impact on the bistable PEH dynamics. First, we develop the analytical model of the P-SSHI circuit associated to the bistable PEH. In a second section, the experimental setup is presented. Finally, the experimental results are presented and we show the extent to which the P-SSHI circuit improves the performance of the harvester compared to the SEH circuit.

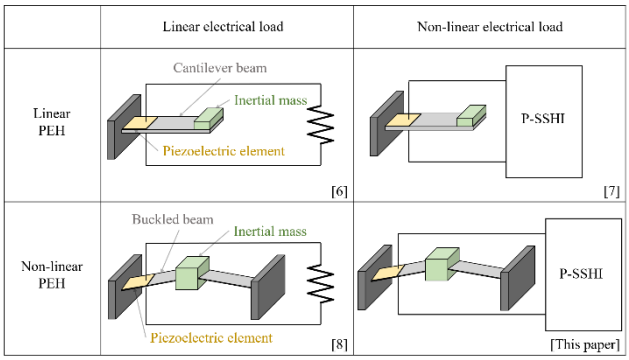

Figure 1: State-of-the-art [6-8] and aim of the present paper: studying the impact of non-linear circuitry on non-linear PEH.

ANALYTICAL MODELLING

As presented in [11], the governing set of differential equations modeling the dynamics of the bistable PEH can be written as follows:

$$\begin{cases} \ddot{x} + \frac{\omega_0}{Q}\dot{x} + \frac{\omega_0^2}{2}\left(\frac{x^2}{x_0^2} - 1\right)x + \frac{2\alpha}{ML}xv_p = \gamma(t) \\ C_p\dot{v_p} = 2\frac{\alpha}{L}x\dot{x} - i_p \end{cases} \quad (1)$$

In (1), x_0, x and α stand respectively for the equilibrium position of the inertial mass, the mass displacement and the piezoelectric force factor. Note, that the waveform of the displacement is experimentally shown to be close to a sine wave and is expressed as $x(t) = x_m \cos(\omega t)$. Assuming that the vibration is sinusoidal, the acceleration amplitude $\gamma(t)$ can be expressed as $\gamma(t) = -\gamma_m \sin(\omega t)$. v_p and i_p are respectively the piezoelectric voltage and current. M, L, C_p, Q and ω_0 are physical parameters of the prototype. They represent the dynamic mass, the length of the beams, the piezoelectric capacitance, the mechanical

quality factor and the natural resonant frequency of the harvester respectively, as summarized in Table 1. Note, that Q and ω_0 correspond to the characteristics of the linear equivalent harvester, obtained for small oscillations of the mass around one of the two equilibrium positions [11]. The simulation of the bistable model (1) may lead to two types of orbits known as intra-well and inter-well motions. In this article, we focused on the inter-well motion due to its interest for energy harvesting.

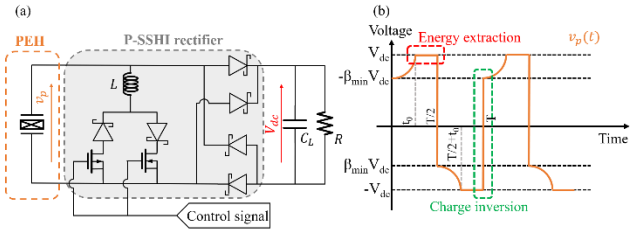

Figure 2: (a) P-SSHI circuit and (b) temporal waveform of the piezoelectric voltage.

The bistable PEH is connected to the P-SSHI circuit presented in Fig. 2.a. During the interval $\left[0,\frac{T}{2}\right]$, the switch, made of the two transistors, is open. The piezoelectric voltage v_p increases until it reaches the rectified voltage V_{dc}. When the piezoelectric voltage becomes equal to V_{dc}, the diode bridge starts conducting, and the electrical energy is extracted from the piezoelectric element. When $t=\frac{T}{2}$, the switch is closed, which connects the inductor L to the piezoelectric capacitance C_p. Because of this L-C loop, the piezoelectric voltage is quickly inversed. Thereafter, another semi-period of vibration starts, and the same process is repeated, as shown in Fig. 2.b.

The waveform of the piezoelectric voltage on a semi-period is illustrated in Fig. 2.b and can be expressed as follows:

$$\begin{cases} v_p(t) = \beta_{min}V_{dc} + \int_0^t \frac{2\alpha x\dot{x}}{C_pL}dt \;\forall t \in [0,t_0] \\ v_p(t) = -V_{dc} \;\forall t \in \left[t_0,\frac{T}{2}\right] \end{cases} \quad (2)$$

$\beta_{min} = \frac{v_p(\frac{T}{2}^+)}{v_p(\frac{T}{2}^-)}$ corresponds to the minimum voltage inversion ratio, as illustrated in Fig. 2.b. Since the piezoelectric voltage is periodic, it can be expressed as a Fourier series. From (2), the expression of the fundamental of the piezoelectric voltage can be obtained:

$$\begin{cases} v_p(t) = a_1\cos(2\omega t) + b_1\sin(2\omega t) \\ a_1 = \frac{\alpha x_m^2}{2LC_p}\frac{1}{1+\frac{\pi}{2r\Omega(1-\beta_{min})}} \\ b_1 = -\frac{\alpha x_m^2}{2LC_p}\frac{2r\Omega\left(\frac{2r\Omega(1-\beta_{min}^2)}{2\pi}+1\right)}{\left((1+\beta_{min})2r\Omega+\pi\right)^2} \end{cases} \quad (3)$$

Where a_1 and b_1 are the first-order Fourier coefficients. Note, that the Fourier coefficients are only expressed for the first order harmonic. Since the mechanical resonator exhibits a filtering behavior, the impact of higher order harmonics of the voltage on the bistable PEH dynamics can be neglected.

Applying the same method as in [8], the electrically-induced damping can be expressed as follows:

$$D_{e_{PSSHI}} = \frac{16\alpha^2 r\Omega\left(\frac{2r\Omega(1-\beta_{min}^2)}{2\pi}+1\right)}{C_p\omega\left((1+\beta_{min})2r\Omega+\pi\right)^2} \quad (4)$$

From this term yields the expression of the damping ratio β_{PSSHI} which corresponds to the ratio between the electrical and the mechanical damping:

$$\beta_{PSSHI} = \frac{x_m^2}{x_0^2}\frac{k_m^2Q}{\Omega}\frac{2r\Omega\left(\frac{2r\Omega(1-\beta_{min}^2)}{2\pi}+1\right)}{\left((1+\beta_{min})2r\Omega+\pi\right)^2} \quad (5)$$
$$with \begin{cases} r = R\,C_p\,\omega_0 \\ \Omega = \omega/\omega_0 \end{cases}$$

Where k_m^2 stands for the electromechanical coupling coefficient. Note, that for another extraction circuit, the Fourier coefficients will be different and thus, the expression of the damping ratio β will change. The first equation of (1) is reformulated to show the damping ratio β_{PSSHI}:

$$\ddot{x} + \frac{\omega_0}{Q}\dot{x}(1+\beta_{PSSHI}) + \frac{\omega_0^2}{2}\left(\frac{x^2}{x_0^2}-1\right)x = \gamma(t) \quad (6)$$

The harmonic balance method is applied to (6) as detailed in [8] and [12], and leads to the equation of the mass displacement amplitude x_m, the critical angular frequency ω_c[1] and the extracted power P_{ext}.

$$\begin{cases} x_m = 2x_0\sqrt{\frac{2}{3}\left(\frac{\omega_c^2}{\omega_0^2}+\frac{1}{2}\right)} \\ \omega_c = \sqrt{\frac{-\omega_0^2+\sqrt{\omega_0^4+\frac{6Q^2\gamma^2}{x_0^2(1+\beta_{PSSHI})^2}}}{4}} \\ P_{ext} = \frac{2M\omega_0\beta_{PSSHI}\omega^2x_0^2}{3Q}\left(1+\frac{2\omega^2}{\omega_0^2}\right) \end{cases} \quad (7)$$

As proven in (7), a larger electrically-induced damping leads to a larger extracted power, but decreases the value of the critical angular frequency, thus limiting the harvesting bandwidth. The electrical efficiency representing the electrical losses during the voltage inversion process of the P-SSHI is expressed as follows:

$$\eta_{elec} = \frac{2\pi}{2\pi+2r\Omega(1-\beta_{min}^2)} \quad (8)$$

Thus, the harvested power P_h can be estimated with:

$$P_h = \eta_{elec}P_{ext} \quad (9)$$

[1] Note that ω_c corresponds to the angular frequency where the inter-well motion of bistable PEH stops existing, as discussed in [12].

EXPERIMENTAL VALIDATION

Bistable piezoelectric energy harvester

Experimental tests were performed on a bistable PEH prototype illustrated in Fig. 3. The bistable PEH is made of an inertial mass and two parallel buckled beams made in steel. In order to convert the mechanical energy into electrical energy, an amplified piezoelectric actuator (APA) made of a stack of lead titano-zirconate has been fixed on the right of the beams. Bistability is induced by applying a buckling force on the beams. Note, that the parameters of the prototype have been experimentally identified on the intra-well motion under a sinusoidal excitation and are presented in Table 1.

Table 1: Prototype parameters.

Parameter	Symbol	Value	Unit
Dynamic mass	M	6.5	g
Buckled beam length	L	35	mm
Piezoelectric capacitance	C_p	1.232	μF
Natural resonant frequency	ω_0	450	$rad.s^{-1}$
Mechanical quality factor	Q	120	-
Electromechanical coupling coefficient	k_m^2	0.060	-

Parallel Synchronized Switch Harvesting on Inductor

As illustrated in Fig. 3, a P-SSHI circuit has been manufactured. The circuit is made of two stages: the switching stage and the rectification stage. As shown in Fig. 2, the switching stage includes an inductor of 0.15 H, two Schottky diodes and two mosfet transistors (a N-channel and a P-channel). The transistors used in the switching stage are ZVN2110GTA for the N-channel and IRFL9110TRPBF for the P-channel. The rectification stage includes 4 Schottky diodes and a filtering capacitor. The Schottky diodes are BAT43 for both the switching and the rectification stages.

Experimental Testbench

To validate the analytical model, an experimental testbench has been set up, as shown in Fig. 3. This fully automated testbench includes a dSpace real time interface, an electromagnetic shaker, a differential laser vibrometer and a programable decade box. The sinusoidal excitation is controlled in closed-loop in order to maintain the vibration amplitude to a constant value. The frequency and the amplitude of the excitation signal as well as the output impedance of the P-SSHI circuit (R in Fig. 2) are controlled with Matlab scripts. The differential vibrometer performs the measurement of displacement and speed of the inertial mass. Voltage followers are used to isolate the APA and the P-SSHI circuit from the input impedance of the acquisition board. For each combination of acceleration, resistance and frequency, the waveforms of the displacement and speed of the mass as well as the piezoelectric voltage and P-SSHI rectified voltage are measured and stored.

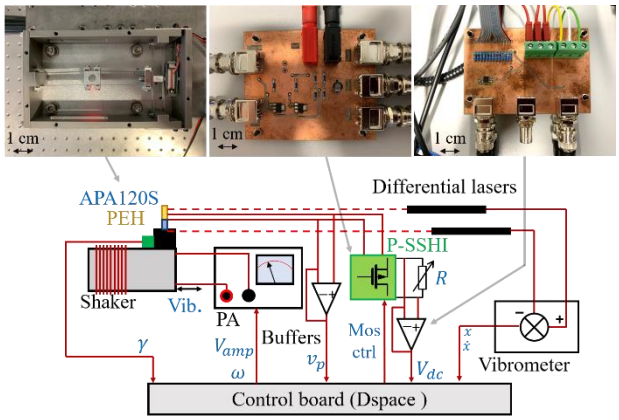

Figure 3: Experimental testbench to test the performances of the bistable PEH prototype connected to the P-SSHI circuit.

Experimental Protocol

The experimental characterization of the PEH connected to the P-SSHI circuit is performed on inter-well motion. The PEH is characterized under a sinusoidal acceleration of amplitude $\gamma_m = 13\ m.s^{-2}$. The frequency is swept from 30 Hz to 80 Hz. These frequency sweeps are performed for 50 load resistances (between 500 Ω and 7 $k\Omega$). The piezoelectric output voltage, P-SSHI rectified voltage, displacement, speed and acceleration waveforms are recorded for each combination of resistance and vibration frequency.

RESULTS & DISCUSSION

Figure 4 illustrates the harvested power and the displacement as a function of the frequency for the bistable PEH connected to the P-SSHI circuit. In both cases, the results are presented for the theory (equations (7) and (8)) and the experiment for three load resistances (from 1 $k\Omega$ to 3 $k\Omega$). Provided that the damping ratio β_{PSSHI} increases as the load resistance increases (5), the harvested power increases for frequencies lower than the critical frequency as shown in Fig. 4.a.

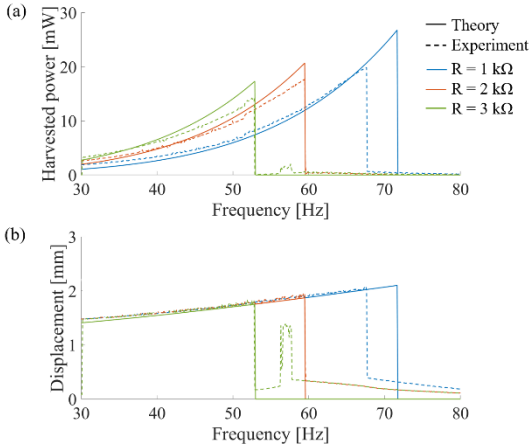

Figure 4: (a) harvested power and (b) displacement for the P-SSHI circuit in theory (solid) and experiment (dash) for R = 1 kΩ (blue), R = 2 kΩ (orange) and R = 3 kΩ (green)

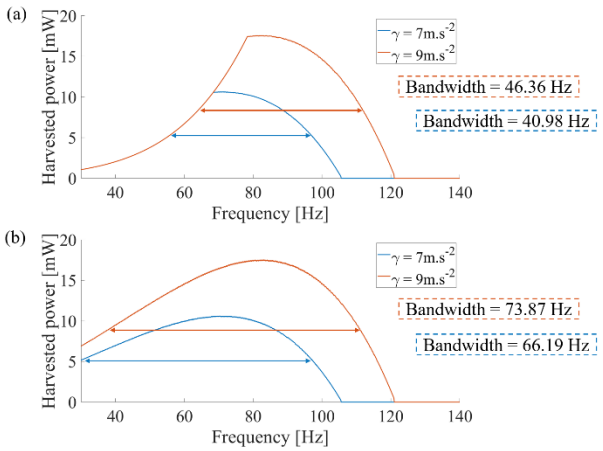

Figure 5: Theoretical power envelope for (a) SEH and (b) P-SSHI circuit with optimal load resistance.

However, the critical frequency decreases due to the large values of the damping ratio ($68\,Hz$ with $R = 1\,k\Omega$ and $52\,Hz$ with $R = 3\,k\Omega$). As illustrated in Fig. 4.b, the displacement for a given frequency is barely impacted by the value of the load resistance, which validates the expression of x_m in (7). The predictions from the proposed model (7) and (9) are in good agreement with the experimental measurements, with less than 20% error on the power and displacement prediction. A slight mismatch can be observed for $R = 1\,k\Omega$, around $70\,Hz$. This mismatch is attributed to mechanical non-linearities (under large displacements) that were not considered in our model (1). Figure 5 shows the theoretical harvested power envelope as a function of the frequency for both the P-SSHI and the SEH circuits. In both cases, the load resistance is finely tuned for each vibration frequency, in order to maximize the harvested power. The harvested power is computed for two acceleration amplitudes ($\gamma = 7\ m.s^{-2}$ and $\gamma = 9\ m.s^{-2}$). From Fig. 5, it can be seen that the bandwidth of bistable PEH is larger with the P-SSHI circuit than with the SEH circuit. As illustrated in Fig. 5.a, the PEH connected to the SEH circuit exhibits a bandwidth of $40.98\,Hz$ under an acceleration amplitude $\gamma_m = 7\ m.s^{-2}$ and a bandwidth of $46.36\,Hz$ for $\gamma_m = 9\ m.s^{-2}$. Fig. 5.b illustrates the power envelope of the bistable PEH connected to the P-SSHI circuit. Under an acceleration amplitude $\gamma_m = 7\ m.s^{-2}$, the PEH exhibits a bandwidth of $66.19\,Hz$. This bandwidth reaches $73.87\,Hz$ when the acceleration amplitude is increased to $\gamma_m = 9\ m.s^{-2}$. Indeed, the P-SSHI interface allows to reach higher electrically induced damping ($\beta_{max} = 4.54$) than the SEH ($\beta_{max} = 1.06$) thus increasing the harvested power under low vibration frequencies and lowering the critical frequency ω_c. Note that the values of β_{max} are given for $f = 48\,Hz$ and $R = 3\,k\Omega$.

CONCLUSION

In this paper, the association of a bistable PEH with a non-linear energy extraction circuit (P-SSHI) has been studied. It was shown, both theoretically and experimentally, that the P-SSHI circuit induces a load-dependent damping on the bistable PEH. Such damping can be electrically-tuned in order to enlarge the bandwidth and the harvested power of the PEH. Thereafter, based on the proposed model, P-SSHI and SEH circuits have been compared. This comparison shows that P-SSHI circuits allow to induce stronger electrically-induced damping value than SEH circuits, thus increasing the harvested power for low frequency vibrations. The obtained bandwidth with the P-SSHI circuit is shown to be 1.6 times larger than with the SEH circuit.

ACKNOWLEDGEMENTS

This work has been supported by the French government, under the Future Investment Program (Programme d'Investissement d'Avenir)

REFERENCES

[1] J. Siang, et al., "Review of vibration-based energy harvesting technology: Mechanism and architectural approach," Int J Energy Res, vol. 42, no. 5, pp. 1866–1893, 2018.

[2] A. Morel, et al., "A unified N-SECE strategy for highly coupled piezoelectric energy scavengers," Smart Mater. Struct., vol. 27, no. 8, p. 084002, 2018.

[3] S. P. Pellegrini, et al., "Bistable vibration energy harvesters: A review," Journal of Intelligent Material Systems and Structures, vol. 24, no. 11, pp. 1303–1312, 2013.

[4] S. M. Shahruz, "Increasing the Efficiency of Energy Scavengers by Magnets," Journal of Computational and Nonlinear Dynamics, vol. 3, no. 4, p. 041001, 2008.

[5] G. K. Ottman, et al., "Adaptive piezoelectric energy harvesting circuit for wireless remote power supply," IEEE Trans. Power Electron., vol. 17, no. 5, pp. 669–676, 2002.

[6] A. Morel, et al., "Resistive and reactive loads' influences on highly coupled piezoelectric generators for wideband vibrations energy harvesting," Journal of Intelligent Material Systems and Structures, vol. 30, no. 3, pp. 386–399, 2019.

[7] Y. C. Shu, et al., "An improved analysis of the SSHI interface in piezoelectric energy harvesting," Smart Mater. Struct., vol. 16, no. 6, pp. 2253–2264, 2007.

[8] Q. Demouron, et al., "Resistive Load Influence on the Power and Bandwidth of Bistable Energy Harvesters", in press, 2022.

[9] T. Huguet, et al., "Bistable vibration energy harvester and SECE circuit: exploring their mutual influence," Nonlinear Dyn, vol. 97, no. 1, pp. 485–501, 2019.

[10] J. Wang, et al., "New insight into piezoelectric energy harvesting with mechanical and electrical nonlinearities," Smart Mater. Struct., vol. 29, no. 4, p. 04LT01, 2020.

[11] T. Huguet, et al., "Parametric analysis for optimized piezoelectric bistable vibration energy harvesters," Smart Mater. Struct., vol. 28, no. 11, p. 115009, 2019.

[12] A. Morel et al., "Simple analytical models and analysis of bistable vibration energy harvesters," Smart Mater. Struct., vol. 31, no. 10, p. 105016, 2022.

CONTACT

*Q. Demouron, quentin.demouron@univ-smb.fr